Dynamics of the photoinduced insulator-to-metal transition in a nickelate film

Vincent Esposito, Laurenz Rettig, Elisabeth M. Bothschafter, Yunpei Deng, Christian Dornes, Lucas Huber, Tim Huber, Gerhard Ingold, Yuichi Inubushi, Tetsuo Katayama, Tomoya Kawaguchi, Henrik Lemke, Kanade Ogawa, Shigeki Owada, Milan Radovic, Mahesh Ramakrishnan, Zoran Ristic, Valerio Scagnoli, Yoshikazu Tanaka, Tadashi Togashi, Kensuke Tono, Ivan Usov, Yoav W. Windsor, Makina Yabashi, Steven L. Johnson, Paul Beaud, and Urs Staub

Citation: Structural Dynamics **5**, 064501 (2018); doi: 10.1063/1.5063530

View online: https://doi.org/10.1063/1.5063530

View Table of Contents: http://aca.scitation.org/toc/sdy/5/6

Published by the American Institute of Physics

Dynamics of the photoinduced insulator-to-metal transition in a nickelate film

Vincent Esposito,[1] Laurenz Rettig,[1,a)] Elisabeth M. Bothschafter,[1] Yunpei Deng,[1] Christian Dornes,[2] Lucas Huber,[2] Tim Huber,[2] Gerhard Ingold,[1] Yuichi Inubushi,[3,4] Tetsuo Katayama,[3,4] Tomoya Kawaguchi,[5] Henrik Lemke,[1] Kanade Ogawa,[3,4] Shigeki Owada,[3,4] Milan Radovic,[1] Mahesh Ramakrishnan,[1] Zoran Ristic,[1,b)] Valerio Scagnoli,[6,7] Yoshikazu Tanaka,[3] Tadashi Togashi,[3,4] Kensuke Tono,[3,4] Ivan Usov,[8] Yoav W. Windsor,[1,a)] Makina Yabashi,[3,4] Steven L. Johnson,[1,2] Paul Beaud,[1] and Urs Staub[1]

[1]*Photon Science Division, Paul Scherrer Institut, 5232 Villigen PSI, Switzerland*
[2]*Institute for Quantum Electronics, ETH Zürich, 8093 Zürich, Switzerland*
[3]*RIKEN SPring-8 Center, Hyogo 679-5148, Japan*
[4]*Japan Synchrotron Radiation Research Institute, Hyogo 679-5198, Japan*
[5]*Department of Materials Science and Engineering, Kyoto University, Kyoto 606-8501, Japan*
[6]*Laboratory for Multiscale Materials Experiments, Paul Scherrer Institut, 5232 Villigen PSI, Switzerland*
[7]*Laboratory for Mesoscopic Systems, Department of Materials, ETH Zurich, 8093 Zurich, Switzerland*
[8]*Science IT, Paul Scherrer Institut, 5232 Villigen PSI, Switzerland*

(Received 28 September 2018; accepted 21 November 2018; published online 6 December 2018)

Material properties can be controlled via strain, pressure, chemical composition, or dimensionality. Nickelates are particularly susceptible due to their strong variations of the electronic and magnetic properties on such external stimuli. Here, we analyze the photoinduced dynamics in a single crystalline $NdNiO_3$ film upon excitation across the electronic gap. Using time-resolved reflectivity and resonant x-ray diffraction, we show that the pump pulse induces an insulator-to-metal transition, accompanied by the melting of the charge order. Finally, we compare our results with similar studies in manganites and show that the same model can be used to describe the dynamics in nickelates, hinting towards a unified description of these photoinduced electronic ordering phase transitions.
https://doi.org/10.1063/1.5063530

I. INTRODUCTION

Transition metal oxides often display complex phase diagrams that originate from the tight interplay between structural, electronic, and magnetic degrees of freedom. The boundaries of these phase diagrams can be tuned by external stimuli, allowing for an effective control of the properties of these functional materials. In particular, epitaxial growth of thin films is commonly used to alter the properties of the bulk material, which leads to the creation of a 2 dimensional electron gas,[1] makes a material polar[2] or even multiferroic,[3] or changes its magnetic structure.[4] Simple perovskite nickelates $RNiO_3$ (R = Y or a Lanthanide ion) belong to a class of materials, which exhibit an insulator-to-metal transition (IMT) (except R = La) and

[a)]Present address: Fritz Haber Institute of the Max Planck Society, 14195 Berlin, Germany.
[b)]Present address: Department of Radiation Chemistry and Physics, VINCA Institute of Nuclear Sciences, Belgrade University, 11000 Belgrade, Serbia.

have an antiferromagnetic insulating ground state. They have a small or even negative charge transfer energy and are considered to belong to charge-transfer insulators.[5] The IMT has been found to be associated with the occurrence of the charge order,[6,7] which leads to a monoclinic structural distortion and an alternation of the size of the NiO_6 octahedra. No orbital order has been found at the Ni sites,[8] which is consistent with the non-collinear magnetic structure found by resonant magnetic x-ray scattering.[9] More recently, it has been theoretically predicted that the charge order is localized in the Ni–O bonds, leading to a splitting of the $d^8\underline{L}$ configuration, where $\underline{L}$ is an oxygen ligand hole, to a $d^8\underline{L}^2$ and d^8 state[10,11] that is associated with the bond order of enlarged and compressed oxygen octahedra.

The IMT in perovskite nickelates is strongly affected by the chemical composition, strain, and dimensional confinement or the proximity to other oxide layers.[12–15] Nickelates are also sensitive to impulsive photoexcitation, and different approaches have been taken to control the electronic or magnetic properties of these materials with short light pulses. The temperature dependent response in $NdNiO_3$ was studied after photoexcitation of the electronic system,[16,17] and different responses were identified in the transient reflectivity signal above and below the ordering temperature. The melting of the antiferromagnetic order was also investigated by time-resolved x-ray diffraction.[18] The reduction of the magnetic order was shown to be linked to a rebalance of the charge on the NiO_6 sites, and the dynamics of the Ni and Nd ions was found to be decoupled during this nonthermal process. The resonant excitation of a substrate vibrational mode with mid-infrared pulses also induces interesting dynamics.[19,20] Such excitation leads to ultrafast modification of the strain, and this was shown to trigger the melting of charge and antiferromagnetic order, as well as the relaxation of the structural distortion, each launched from the interface with different propagation velocities.[21]

Recent ultrafast studies of the photoinduced IMT in half-doped manganites proposed a unified view of the dynamics following photoexcitation of the electronic system. The underlying electronic order was shown to be destroyed on a fast timescale and to trigger the subsequent structural dynamics.[22] To describe the fluence dependence of the phase transition, a time-dependent order parameter was introduced. Even though this model nicely describes the data, it remains to be shown whether this model is applicable to other photoinduced phase transitions that have a different electronic origin.

In this study, we use the pump-probe approach to explore the photoinduced insulator-to-metal transition in an epitaxially grown $NdNiO_3$ film after direct excitation of the electronic system. The sample is excited with short 800 nm pulses, corresponding to a transition across the gap in the antibonding e_g band of nickel.[23] The transient dynamics are studied using two different approaches. The temperature and fluence dependence of the transient reflectivity is measured at a wavelength of 800 nm, and a more direct view on the time evolution of the long range charge order is provided by time-resolved resonant x-ray diffraction.

II. EXPERIMENTAL DETAILS

The 60 nm thick $NdNiO_3$ thin film was grown by pulsed laser deposition on a $NdGaO_3$ substrate with (110) surface orientation (using the *Pbnm* space group) as described elsewhere.[24] The sample was characterized at the X04SA surface diffraction beamline at the Swiss Light Source at PSI. The charge order can be directly measured by probing reflections of the type (0*kl*) (in *Pbnm* symmetry), with k and l odd, at the Ni K edge resonance.[7,8] The ordering temperature measured *via* the disappearance of the resonant contribution in the $(01\bar{3})$ is $T_{CO} = 155$ K (Fig. 1), about 50 K below the bulk value and consistent with that of other $NdNiO_3$ thin films.[24]

The time-resolved x-ray diffraction experiments were carried out at beamline 3 of the SACLA free electron laser (FEL).[25,26] The x-ray energy was set to the Ni K edge, granting sensitivity to the charge ordering pattern in the low temperature phase. The x-ray beam was focused with a KB mirror system to 50×40 μm^2 (full width at half maximum), and the 800 nm pump laser was focused to be 250×250 μm^2. Taking into account the incident angles (10° for the pump laser and 5° for the x-ray probe) of the beams, the footprint of the x-ray beam was about 2 times smaller than the laser beam, ensuring homogeneous in-plane excitation. The

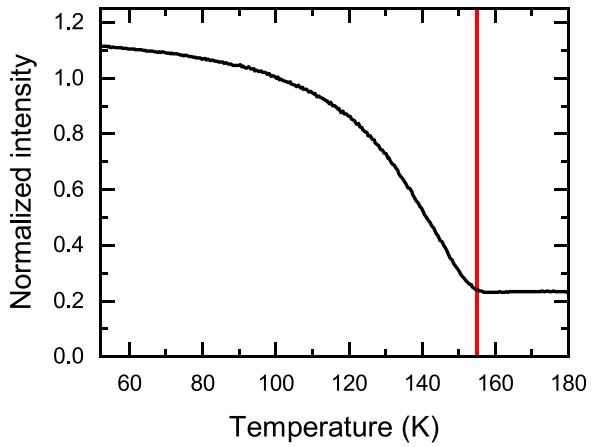

FIG. 1. Temperature dependence upon warming of the $(01\bar{3})$ reflection at resonance ($E = 8.345$ keV). The diffracted intensity is normalized to the value at 100 K, and the vertical line indicates the ordering temperature $T_{CO} = 155$ K, about 50 K below that of the bulk material.

diffracted signal was monochromatized with a Cu (111) analyzer by choosing the (222) reflection that results in $2\theta \approx 90°$ at the nickel K edge and measured using a yttrium aluminum perovskite (YAP) detector. The energy was optimized to the maximum of the $(01\bar{3})$ reflection resonance that has a very similar energy dependence to (015) at 8.345 keV.[7] Despite being at resonance, the background remains actually very small because the fluorescence has a different energy and is therefore suppressed by the analyzer crystal. Because the monochromator (analyzer) is placed downstream from the I_0 monitor, we are, however, very sensitive to the shot-to-shot intensity jitter of that particular spectral component. The sample temperature was kept at about 100 K, well below the charge ordering temperature, by means of a nitrogen cryoblower. Due to the jitter between the pump and probe pulses, the overall time-resolution was about 700 fs, significantly lower than the cross-correlation between the optical pump and the x-ray probe of 50 fs. Note that a timing diagnostic tool, allowing us to correct for the jitter, was installed at the beamline in the meantime.[27]

Time-resolved reflectivity was performed with an 800 nm probe at a repetition rate of 2 kHz, alternating between pumped and unpumped shots, in order to correct for slow drifts in the laser and electronics. The pump and probe beams were produced by splitting the output of a regenerative amplifier system seeded by a Ti:S oscillator. The pump was focused to 480×550 μm^2 and the probe to 110×110 μm^2, guaranteeing homogeneous excitation. The time resolution, measured from the cross-correlation of the two beams in a $Ba(BO_2)_2$ crystal, was about 80 fs. The sample was placed in a cryostat coupled to a close-loop helium compressor, allowing temperature stabilization down to approximately 5 K. The reflectivity was measured at normal incidence using a fast photodiode and gated by a boxcar integrator.

III. RESULTS

A. Transient optical reflectivity

1. Temperature dependence

The temperature dependence of the 800 nm transient reflectivity changes at a fluence of 0.8 mJ cm^{-2} is shown in Fig. 2. For the sake of clarity, only a few selected temperatures are displayed out of a larger dataset. Very different responses are observed when exciting the sample above or below T_{CO}. Below the ordering temperature, the reflectivity decreases promptly upon excitation followed by a slower relaxation towards a metastable state. The reduced reflectivity originates from a transfer of the spectral weight to lower frequencies linked to the increased DC conductivity after photo-doping. Above T_{CO}, a slight and prompt increase in reflectivity is observed and decays within a few hundreds of femtoseconds back to the equilibrium value.

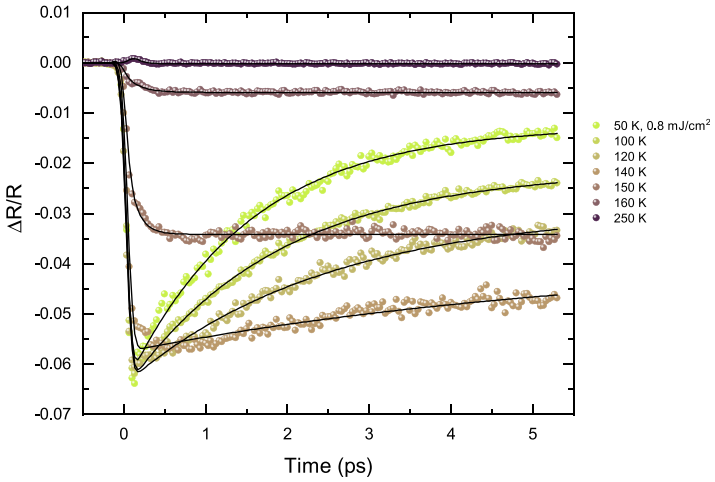

FIG. 2. Temperature dependence of the transient reflectivity in $NdNiO_3$. Major changes are observed around the critical temperature of $T_{CO} = 150$ K. The black lines are fit with Eq. (1).

This initial increase in reflectivity is consistent with the response of a metallic state,[28] but its rapid recovery resembles the dynamics observed in semi-conductors.[29] Finally, an intermediate regime is observed at the transition temperature with a prompt decrease followed by a slower decrease after which reflectivity either is constant or recovers, depending on the starting temperature.

This behaviour is best seen when fitting the data with a single exponential relaxation

$$\frac{\Delta R}{R} = 0.5 \cdot \left(erf\left(\frac{t - t_0}{\sigma}\right) + 1 \right) \cdot \left(A e^{-\frac{t-t_0}{\tau}} + c \right). \tag{1}$$

The first part simulates the time-dependent excitation profile with a duration of $\sigma = 80$ fs and arrival time t_0, with $erf(x)$ being the error function. The initial reflectivity change is given by the amplitude A and the timescale of the recovery by τ, and the constant c accounts for the long-lived transient that lasts well beyond 5 ps. The fitted curves are overlaid to the data in Fig. 2 (black lines). The fitted parameters are reported in Fig. 3. They all display a sharp discontinuity in their respective trend around the critical temperature T_{CO}. In particular, the amplitude A changes its sign at the transition. The recovery slows down as the temperature is increased in the insulating phase and becomes suddenly extremely fast in the metallic state. Close to the critical temperature, the fast drop in reflectivity is followed by a further reduction in reflectivity in a time period of about 0.5 ps and the recovery is suppressed. These additional features lead to the increased error bars in Fig. 3, visualizing the difficulties in fitting the data with this simple model. These effects may be caused by the thermalization between co-existing metallic and insulating domains in the hysteretic window.[30] Additionally, the pump penetration depth is of the order of the film thickness and the top part of the film is thus more excited than deeper layers. Close to the critical temperature, this increased excitation may trigger the transition to the high temperature phase and further reduction of reflectivity can also be attributed to thermalization between melted and unmelted layers. Note that the physical meaning of the parameters may change at the phase transition, in particular, in the regime where the two phases coexist. For example, while the time constant τ always represents a thermalization time, it may not always be between the same subsystems, i.e., thermalization between different domains in the hysteretic window may modify the behavior of this parameter.

It is worth noting that no coherent oscillations are observed in the low temperature phase, as opposed to the charge ordered manganites.[31–33] A structural distortion occurs nonetheless at the ordering temperature, leading to a lowering of the crystal symmetry from orthorhombic to monoclinic. In the ultrafast regime, structural dynamics are decoupled between the small atomic motions within the unit cell and the change in the unit cell shape and/or size.[34] The first part is

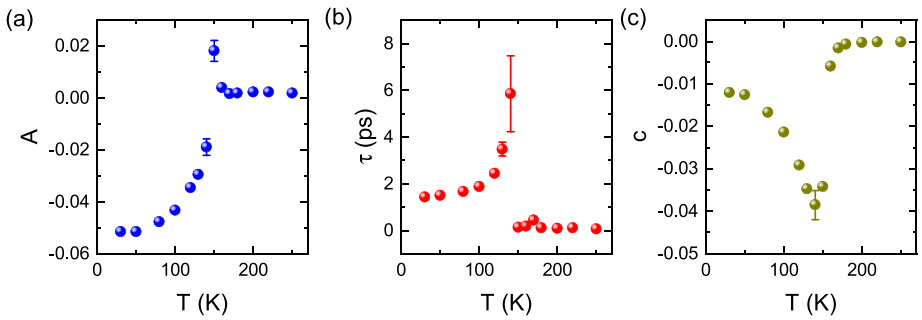

FIG. 3. Parameters from the fit of Eq. (1) to the data in Fig. 2 as a function of temperature. The transition around 150 K is clearly visible in all three parameters.

generally faster and carried by coherent optical phonons, while the second part is limited by the speed of sound in the material. In nickelates, the main structural motion involves the expansion/contraction of the oxygen octahedra. This motion is driven by breathing modes, whose frequency cannot be resolved with the experimental time resolution of 80 fs but should eventually lead to the displacement of the heavier rare-earth ions, at lower frequencies. The amplitude of the rare-earth displacements during the thermodynamic transition is comparable to that in manganites,[35] where a pronounced coherent oscillation is observed upon photoexcitation. The absence of coherent oscillation at low frequency in the reflectivity is thus puzzling. Several hypotheses can, however, explain our observations. The phonon may be overdamped, or the motion of the rare-earth ions may not be strongly coupled to the oxygen octahedral breathing mode and only follow the slower change of the unit cell involving the monoclinic to orthorhombic transition, which has been reported upon mid-infrared excitation.[21] Finally, the rare-earth motion may only induce small variation of the refractive index. The transient reflectivity signal would then be very little sensitive to those motions.

A similar pump-probe study at 760 nm has been reported on a 150 nm $NdNiO_3$ film grown on a (100) silicon substrate, corresponding to the (110) orthorhombic direction.[16] In this study, the reflectivity was found to increase after excitation in both the insulating and the metallic phases. Moreover, a crossover from a double to a single exponential recovery is observed at the transition. Our data are thus consistent with the reported behavior in the metallic state but differ significantly in the ordered phase. This might be caused by the microstructure difference of films grown on the silicon substrate, which have much larger strain compared to films grown on orthorhombic perovskite oxides.[36] Nickelates are indeed extremely sensitive to strain,[15] and for large strains, it is expected that the films break up in smaller domains.[36] The increase in the number of domain walls, which possibly remain conductive,[30] could lead to a different overall response in the insulating state.

2. Fluence dependence

The fluence dependent transient reflectivity above and below the ordering temperature is shown in Fig. 4. Panel (a) shows the transient reflectivity at 100 K, well below the ordering temperature. At low fluence, the prompt intensity drop is followed by a slower relaxation. For fluences above 2 mJ cm^{-2}, the initial drop saturates to about –10%. At this point, no more recovery is observed within the first 5 ps and the reflectivity seems actually to drop even further on longer timescales. Based on the optical properties at 800 nm (1.55 eV) for $NdNiO_3$ grown on $NdGaO_3$ (110), a 10% reduction in reflectivity is expected when heating through the transition.[37] The saturation of the transient reflectivity drop at this value clearly indicates the completion of a photoinduced IMT in this material.

For fluences above 1.1 mJ cm^{-2}, the reflectivity drops further on a 0.5 ps timescale. These dynamics resemble those close to the critical temperature (Fig. 2), possibly indicating the presence of phase co-existence. Because of the inhomogeneities in the film, it is, indeed, possible that parts of the film undergo the transition at a lower fluence.

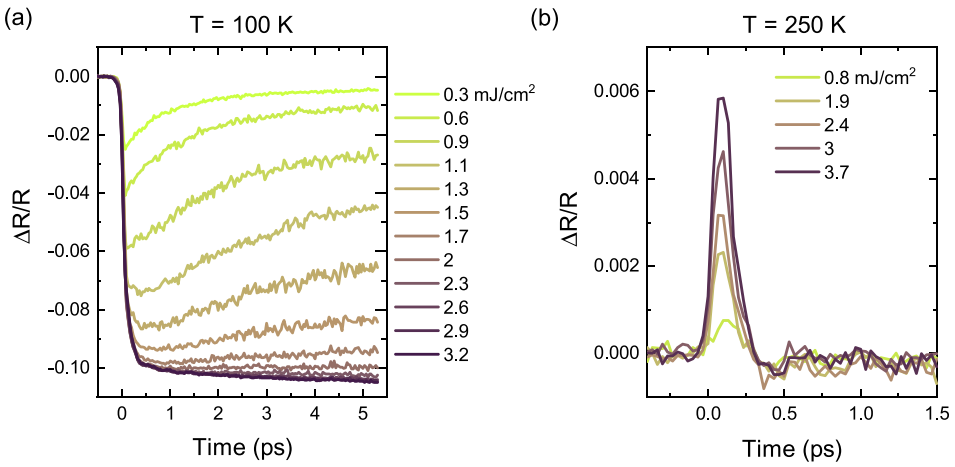

FIG. 4. Transient 800 nm reflectivity as a function of fluence for temperature below (100 K) (a) and above (250 K) (b) the ordering temperature.

Close to the critical temperature, the fluence needed to induce the transition seems to decrease. Indeed, the data at 140 K and 150 K of the transient reflectivity (Fig. 2) resemble the curves around the critical fluence at 100 K. The fluence of 0.8 mJ cm^{-2} appears to be large enough to induce the transition at these temperatures. At high temperature, the initial increase in reflectivity scales linearly with fluence [Fig. 4(b)] and the recovery time of a couple of 100 fs does not show any significant fluence dependence.

The dynamics above the critical fluence resembles closely those observed upon strong resonant excitation of a substrate lattice mode.[19] This type of excitation was shown to also induce the melting of the charge order and the relaxation of the structural distortion, demonstrating a transition to a metastable state resembling the high temperature phase.[20,21] The fact that the same response is observed here indicates that the same transient state is being induced.

B. Resonant x-ray diffraction

Resonant x-ray diffraction provides a more quantitative and direct view of this IMT, as it can directly probe the underlying electronic ordering phenomena. In Fig. 5, an energy scan of the $(01\bar{3})$ forbidden reflection above and below T_{CO} is shown. The reflections of the type $(0kl)$ with k and l odd are forbidden in the high temperature orthorhombic symmetry and are directly sensitive to the charge order at resonance in the low temperature phase. For $T > T_{CO}$ and far

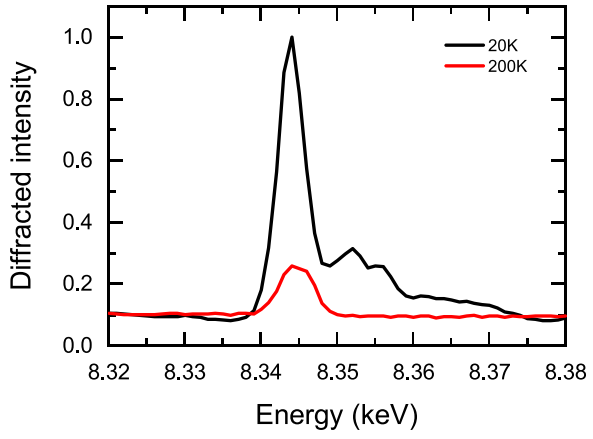

FIG. 5. Energy-dependent XRD intensity of the $(01\bar{3})$ forbidden reflection above and below T_{CO}. The intensity is normalized to the maximal intensity of the low temperature scan.

from the nickel K edge (8.33 keV), the peak intensity is almost zero and the small energy independent contribution may originate from a slight distortion of the orthorhombic structure, possibly stabilized by strain. There is also a small contribution from the substrate, possibly multiple scattering, as verified by measuring a bare $NdGaO_3$ crystal. At resonance, there is a small orbital contribution left as studied in detail in Ref. 8. Below T_{CO}, the resonant contribution is significantly enhanced due to the charge ordering at the NiO_6 octahedra.[7,8] The high temperature contribution to the reflection intensity is about 25% to the one at 100 K.

The dynamics of the $(01\bar{3})$ reflection as a function of time is shown in Fig. 6(a). As stated in Sec. II, this reflection at resonance is a direct measure of the long-range order of the charge order. A fast reduction of intensity is observed immediately after photo-excitation with the pump pulse, evidencing a prompt reduction of the charge order. Above 3.3 mJ cm^{-2}, the intensity drop saturates to about 30% of its maximum intensity. This corresponds closely to the remaining diffraction intensity observed in the high temperature phase (Fig. 5), demonstrating the complete melting of the charge ordered state.

In Fig. 6(b), the intensity drop averaged between 4 and 6 ps is plotted as a function of the incoming fluence. In the equilibrium phase, the enhanced resonant contribution of this forbidden peak is an order parameter of the charge ordered phase. Assuming that the electronic system has thermalized, the transient intensity of $(01\bar{3})$ can be considered as a valid order parameter square of the electronic order. The intensity of the reflection as a function of fluence is thus described with a continuous Landau-like order parameter, a model based on the description of the charge order dynamics in a manganite.[22] As the excitation depth (≈50 nm) is comparable to the film thickness and is much smaller than the x-ray penetration length, we account for the depth-dependent excitation profile by splitting the sample in $N = 60$ layers. Each layer contributes to the diffracted intensity according to its excitation density $n_i = n_0 e^{-z/z_0}$, where z_0 is the penetration depth of the laser. The diffracted intensity is then given by

$$I = \eta^2, \quad \text{with } \eta = \frac{1}{N}\sum_i^N \begin{cases} \left(1 - \frac{n_i}{n_c}\right)^{\gamma}, & \text{if } n_i < n_c \\ 0, & \text{otherwise.} \end{cases} \tag{2}$$

An additional scaling factor and an offset are used to account for the remaining intensity at high temperature and are taken from the intensity above and below the ordering temperature in

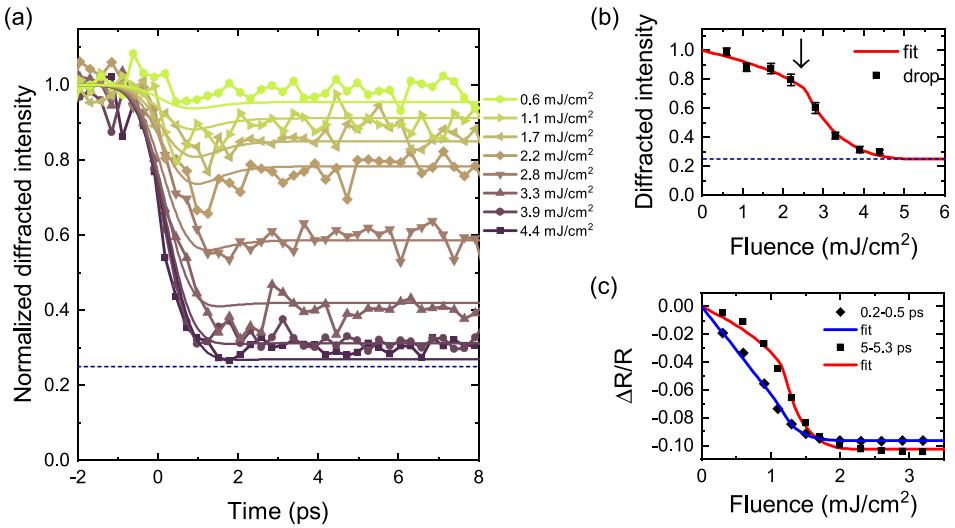

FIG. 6. (a) Time dependence of the $(01\bar{3})$ reflection after excitation with 800 nm pulses at 100 K. The horizontal dashed line indicates the intensity of the peak above the ordering temperature. (b) Average normalized intensity between 4 and 6 ps as a function of fluence. The black arrow indicates the fluence corresponding to the critical energy density at the surface ($f_c = 2.5$ mJ cm^{-2}). (c) Average reflectivity drops at early and later times after excitation. The data are fitted with Eq. (2).

Fig. 5. The fit yields a critical energy density n_c of $= 343 \pm 7$ J cm^{-3} and an exponent γ of $= 0.15 \pm 0.02$. In Fig. 6(c), the reflectivity drop extracted from Fig. 4(a) is reported for early and later delays after excitation. Just after excitation, the reflectivity drop is linear. At later delays, its response qualitatively resembles that of the charge order. The fit of these curves with Eq. (2) yields a critical energy density of $n_c = 165 \pm 5$ J cm^{-3} and $\gamma = 0.18 \pm 0.02$. The difference between the critical energy densities found for the two experiments may be intriguing. The critical energy density in the optical experiment corresponds to a critical fluence at the surface of 1.2 mJ cm^{-2}, which is compatible with that found for the melting of the magnetic order.[18] The critical energy density for the melting of the charge order is approximately twice as large. The determination and comparison of fluences across different experiments are, however, a challenging task, as the uncertainties in the laser power and beam size measurements can be quite large. Moreover, the different pump pulse duration may also be responsible for these differences.

In manganites, the photoinduced melting of the charge order and its associated dynamics were successfully described with a time-dependent order parameter.[22] Starting from Eq. (2), we account for the electron-lattice thermalization by considering the time-evolution of the energy deposited in the electronic system: $n_i \rightarrow n_i(t)$. Indeed after excitation, the excess energy dissipates into the lattice until a common temperature is reached. Below the critical energy density n_c, this dissipation leads to a partial recovery of the charge order and its order parameter. Above n_c, the transition occurs and the system remains trapped in an electronically disordered metastable state. It was proposed that this description could apply to other photoinduced transitions as well. We have thus applied this model to the case of nickelates. We have considered the empirical evolving energy density $n_i(t)$ that was also used for the manganites[22]

$$n_i(t) = (n_{i0} - \alpha n_c)e^{-t/\tau} + \alpha n_c, \tag{3}$$

with

$$\alpha = 1 - \left(1 - \frac{n_{i0}}{n_c}\right)^{2\gamma} \tag{4}$$

where n_{i0} is the energy deposited by the laser at $t = 0$ in layer i, τ is the timescale of the thermalization, and γ is a parameter that determines the amount of order in the metastable state. This model is a time-dependent generalization of the model proposed in Eq. (2), where a partial exponential relaxation with time constant τ is considered. Only three free parameters are used to fit all curves simultaneously (n_c, τ, and γ), and the resulting fits are overlaid to the data in Fig. 6(a). The fit results in very similar values for the parameters n_c and γ compared to Eq. (2) ($n_c = 349 \pm 3$ Jcm^{-3}; $\gamma = 0.168 \pm 0.006$). The time constant is found to be $\tau = 0.53 \pm 0.09$ ps, of the order of the time resolution of the experiment. From the reasonable good agreement between the model and the data, we conclude that the time-dependent order parameter model also describes the melting of charge order in nickelates, despite the different electronic origins of the phase transitions and very different conductivity changes in the static case. Note that whereas the electronic phase transition in half doped manganites is accompanied by charge and orbital ordering phenomena, the orbital degree of freedom does not play a crucial role in nickelates. Therefore, this behaviour hints at a possible universality of the time dependent order parameter approach.

IV. CONCLUSION

In summary, we have shown that the temperature-dependent phase transition is clearly identifiable in the reflectivity changes. The transient response is consistent with an insulating phase at low temperature and with a metallic state above the ordering temperature. The fluence-dependent transient reflectivity reveals the completion of a photoinduced insulator-to-metal transition above a certain threshold. A detailed investigation of the charge order dynamics

with resonant x-ray diffraction shows indeed a melting of the charge order above a critical fluence, confirming the photoinduced phase transition. The description of the data with a time-dependent order parameter model demonstrated that, as for manganites, these dynamics can be well described using exclusively the absorbed energy.

ACKNOWLEDGMENTS

This work was supported by the Swiss National Science Foundation and its National Centers of Competence in Research in Molecular Ultrafast Science and Technology (NCCR MUST). E.M.B. acknowledges funding from the European Community's Seventh Framework Programme (FP7/2007-2013) under Grant Agreement No. 290605 (PSI-FELLOW/COFUND). The time-resolved x-ray experiments were performed under the approval of the Japan Synchrotron Radiation Research Institute (JASRI Proposals Nos. 2014A8006 and 2015B8009).

[1]A. Ohtomo and H. Hwang, Nature **427**, 423 (2004).
[2]J. H. Haeni, P. Irvin, W. Chang, R. Uecker, P. Reiche, Y. L. Li, S. Choudhury, W. Tian, M. E. Hawley, B. Craigo *et al.*, Nature **430**, 758 (2004).
[3]J. A. Mundy, C. M. Brooks, M. E. Holtz, J. A. Moyer, H. Das, A. F. Rébola, J. T. Heron, J. D. Clarkson, S. M. Disseler, Z. Liu *et al.*, Nature **537**, 523 (2016).
[4]Y. W. Windsor, S. W. Huang, Y. Hu, L. Rettig, A. Alberca, K. Shimamoto, V. Scagnoli, T. Lippert, C. W. Schneider, and U. Staub, Phys. Rev. Lett. **113**, 167202 (2014).
[5]T. Mizokawa, H. Namatame, A. Fujimori, K. Akeyama, H. Kondoh, H. Kuroda, and N. Kosugi, Phys. Rev. Lett. **67**, 1638 (1991).
[6]J. Alonso, J. García-Muñoz, M. Fernández-Díaz, M. Aranda, M. Martínez-Lope, and M. Casais, Phys. Rev. Lett. **82**, 3871 (1999).
[7]U. Staub, G. I. Meijer, F. Fauth, R. Allenspach, J. G. Bednorz, J. Karpinski, S. M. Kazakov, L. Paolasini, and F. d'Acapito, Phys. Rev. Lett. **88**, 126402 (2002).
[8]V. Scagnoli, U. Staub, M. Janousch, A. M. Mulders, M. Shi, G. I. Meijer, S. Rosenkranz, S. B. Wilkins, L. Paolasini, J. Karpinski *et al.*, Phys. Rev. B **72**, 155111 (2005).
[9]V. Scagnoli, U. Staub, A. M. Mulders, M. Janousch, G. I. Meijer, G. Hammerl, J. M. Tonnerre, and N. Stojic, Phys. Rev. B **73**, 100409 (2006).
[10]T. Mizokawa, D. I. Khomskii, and G. A. Sawatzky, Phys. Rev. B **61**, 11263 (2000).
[11]S. Johnston, A. Mukherjee, I. Elfimov, M. Berciu, and G. A. Sawatzky, Phys. Rev. Lett. **112**, 106404 (2014).
[12]A. Boris, Y. Matiks, E. Benckiser, A. Frano, P. Popovich, V. Hinkov, P. Wochner, M. Castro-Colin, E. Detemple, V. Malik *et al.*, Science **332**, 937 (2011).
[13]A. Frano, E. Schierle, M. W. Haverkort, Y. Lu, M. Wu, S. Blanco-Canosa, U. Nwankwo, A. V. Boris, P. Wochner, G. Cristiani *et al.*, Phys. Rev. Lett. **111**, 106804 (2013).
[14]S. Middey, J. Chakhalian, P. Mahadevan, J. Freeland, A. J. Millis, and D. Sarma, Annu. Rev. Mater. Res. **46**, 305 (2016).
[15]S. Catalano, M. Gibert, J. Fowlie, J. Íñiguez, J.-M. Triscone, and J. Kreisel, Rep. Prog. Phys. **81**, 046501 (2018).
[16]P. Ruello, S. Zhang, P. Laffez, B. Perrin, and V. Gusev, Phys. Rev. B **76**, 165107 (2007).
[17]P. Ruello, S. Zhang, P. Laffez, B. Perrin, and V. Gusev, Phys. Rev. B **79**, 094303 (2009).
[18]A. D. Caviglia, M. Först, R. Scherwitzl, V. Khanna, H. Bromberger, R. Mankowsky, R. Singla, Y.-D. Chuang, W. S. Lee, O. Krupin *et al.*, Phys. Rev. B **88**, 220401 (2013).
[19]A. D. Caviglia, R. Scherwitzl, P. Popovich, W. Hu, H. Bromberger, R. Singla, M. Mitrano, M. C. Hoffmann, S. Kaiser, P. Zubko *et al.*, Phys. Rev. Lett. **108**, 136801 (2012).
[20]M. Först, A. D. Caviglia, R. Scherwitzl, R. Mankowsky, P. Zubko, V. Khanna, H. Bromberger, S. B. Wilkins, Y.-D. Chuang, W. S. Lee *et al.*, Nat. Mater. **14**, 883 (2015).
[21]M. Först, K. R. Beyerlein, R. Mankowsky, W. Hu, G. Mattoni, S. Catalano, M. Gibert, O. Yefanov, J. N. Clark, A. Frano *et al.*, Phys. Rev. Lett. **118**, 027401 (2017).
[22]P. Beaud, A. Caviezel, S. Mariager, L. Rettig, G. Ingold, C. Dornes, S. Huang, J. Johnson, M. Radovic, T. Huber *et al.*, Nat. Mater. **13**, 923 (2014).
[23]M. K. Stewart, J. Liu, M. Kareev, J. Chakhalian, and D. N. Basov, Phys. Rev. Lett. **107**, 176401 (2011).
[24]R. S. Dhaka, T. Das, N. C. Plumb, Z. Ristic, W. Kong, C. E. Matt, N. Xu, K. Dolui, E. Razzoli, M. Medarde *et al.*, Phys. Rev. B **92**, 035127 (2015).
[25]T. Ishikawa, H. Aoyagi, T. Asaka, Y. Asano, N. Azumi, T. Bizen, H. Ego, K. Fukami, T. Fukui, Y. Furukawa *et al.*, Nat. Photonics **6**, 540 (2012).
[26]K. Tono, T. Togashi, Y. Inubushi, T. Sato, T. Katayama, K. Ogawa, H. Ohashi, H. Kimura, S. Takahashi, K. Takeshita *et al.*, New J. Phys. **15**, 083035 (2013).
[27]T. Katayama, S. Owada, T. Togashi, K. Ogawa, P. Karvinen, I. Vartiainen, A. Eronen, C. David, T. Sato, K. Nakajima *et al.*, Struct. Dyn. **3**, 034301 (2016).
[28]R. W. Schoenlein, W. Z. Lin, J. G. Fujimoto, and G. L. Eesley, Phys. Rev. Lett. **58**, 1680 (1987).
[29]S. Gupta, J. F. Whitaker, and G. A. Mourou, IEEE J. Quantum Electron. **28**, 2464 (1992).
[30]K. W. Post, A. S. McLeod, M. Hepting, M. Bluschke, Y. Wang, G. Cristiani, G. Logvenov, A. Charnukha, G. X. Ni, P. Radhakrishnan *et al.*, Nat. Phys. **14**, 1056 (2018).
[31]D. Lim, V. K. Thorsmølle, R. D. Averitt, Q. X. Jia, K. H. Ahn, M. J. Graf, S. A. Trugman, and A. J. Taylor, Phys. Rev. B **71**, 134403 (2005).
[32]H. Matsuzaki, H. Uemura, M. Matsubara, T. Kimura, Y. Tokura, and H. Okamoto, Phys. Rev. B **79**, 235131 (2009).

[33]A. Caviezel, U. Staub, S. L. Johnson, S. O. Mariager, E. Möhr-Vorobeva, G. Ingold, C. J. Milne, M. Garganourakis, V. Scagnoli, S. W. Huang *et al*., Phys. Rev. B **86**, 174105 (2012).
[34]V. Esposito, L. Rettig, E. Abreu, E. M. Bothschafter, G. Ingold, M. Kawasaki, M. Kubli, G. Lantz, M. Nakamura, J. Rittman *et al*., Phys. Rev. B **97**, 014312 (2018).
[35]J. Garcia-Munoz, M. Aranda, J. Alonso, and M. Martinez-Lope, Phys. Rev. B **79**, 134432 (2009).
[36]P. Laffez, R. Retoux, P. Boullay, M. Zaghrioui, P. Lacorre, and G. Van Tendeloo, Eur. Phys. J.-Appl. Phys. **12**, 55 (2000).
[37]J. Ruppen, J. Teyssier, O. E. Peil, S. Catalano, M. Gibert, J. Mravlje, J.-M. Triscone, A. Georges, and D. van der Marel, Phys. Rev. B **92**, 155145 (2015).